Received: 25 October 2020 | Revised: 3 December 2020 | Accepted: 18 December 2020

DOI: 10.1002/er.6378

RESEARCH ARTICLE

INTERNATIONAL JOURNAL OF ENERGY RESEARCH WILEY

# Optoelectronic and transport properties of $Rb/Cs_2TeI_6$ defective perovskites for green energy applications

**Malak Azmat Ali**[1] | **Ali H. Reshak**[2,3,4] | **Ghulam Murtaza**[5] | **Murefahmana AL-Anazy**[6] | **Hind Althib**[7,8] | **Tahani H. Flemban**[7,8] | **Jiri Bila**[3]

[1]Department of Physics, Government Post Graduate Jahanzeb College, Saidu Sharif, Pakistan

[2]Physics Department, College of Science, University of Basrah, Basrah, Iraq

[3]Department of Instrumentation and Control Engineering, Faculty of Mechanical Engineering, CTU in Prague, Prague, Czech Republic

[4]Center of Excellence Geopolymer and Green Technology, School of Material Engineering, University Malaysia Perlis, Kangar, Malaysia

[5]Materials Modeling Lab, Department of Physics, Islamia College Peshawar, Peshawar, Pakistan

[6]Department of Chemistry, College of Science, Princess Nourah Bint Abdulrahman University, Riyadh, Saudi Arabia

[7]Basic and Applied Scientific Research Center, Imam Abdulrahman Bin Faisal University, Dammam, Saudi Arabia

[8]Department of Physics, College of Science, Imam Abdulrahman Bin Faisal University, Dammam, Saudi Arabia

**Correspondence**
Ali H. Reshak, Physics Department, College of Science, University of Basrah, Basrah, Iraq.
Email: maalidph@yahoo.co.uk

**Summary**

Lead content in perovskite solar cells and other applications is toxic for human health and environment. Therefore, the search alternate materials are required of present era. In this article, we presented physical properties of $Rb/Cs_2TeI_6$ defective perovskites for possible solar cell and thermoelectric applications. These compounds were found to be stable in perovskite structure. The band gaps were calculated in close contact to experiments. The optical properties were computed in term of dielectric function, refractive index and optical conductivity. These properties explored suitability of $Rb/Cs_2TeI_6$ perovskites for solar cell applications. Also, the high figure of merit (0.687 for $Rb_2TeI_6$ and 0.682 for $Cs_2TeI_6$ at 1000 K) confirmed position of these compounds in family of efficient thermoelectric materials.

**KEYWORDS**

defective perovskites, figure of merit, optical conductivity, solar cell applications, thermoelectric materials

## 1 | INTRODUCTION

Despite maximum reported efficiency,[1] the lead halide perovskites are toxic to be used in solar cells and thermoelectric generators because the lead contents of these compounds may cause symptoms ranging from the loss of function of neurons to death depending upon the amount and exposure time.[2] Average exposure levels in children leaving near the plants of lead solar cells and battery in developing countries are four times of the level established by the World Health Organization.[3] Therefore, it is highly recommended to replace the solar cells contents by environmentally friendly materials.

The half of B site cation removed in $ABX_3$ perovskites may be alternative of lead halide perovskites. These materials are represented by $A_2BX_6$ and termed as defective perovskites. A number of researchers carried investigations on materials in $A_2BX_6$ group and reported them

  

as excellent absorber to be used in solar cell applications.[4-12] Also materials of this group have been reported with excellent thermoelectric properties.[4-7] Among $A_2BX_6$ defective perovskites, $Rb/Cs_2TeI_6$ compounds have not been studies at experimental or theoretical level for solar cells and thermoelectric applications. Abriel[13] prepared $Rb_2TeI_6$ and reported it with cubic $A_2BX_6$ at 340 K. Sidey et al[14] reported lattice constant of $Cs_2TeI_6$ as 11.700 Å from his experiment. Peresh et al[15] also reported the cubic structure of $Rb_2TeI_6$ along with $Cs_2TeI_6$. They reported the band gap of $Rb_2TeI_6$ as 1.4 eV and as $Cs_2TeI_6$ 1.5 eV from their experiment. Brik and Kityk[16] calculated lattice constant for $Cs_2TeI_6$ from their developed analytical technique. Rahim et al[17] also calculated the lattice constant for $Cs_2TeI_6$ at analytical level. Up till now, the optical and thermoelectric properties neither reported experimentally nor theoretically while electronic properties were not studied theoretically. Therefore, it will be very interesting to investigate the optical and thermoelectric properties further.

In the present article, we reported the density functional theory based results of lattice parameters, optical and thermoelectric spectra, and electronic properties in term of band structure and density of states for $Rb/Cs_2TeI_6$ defective perovskites. The new results on these compounds can cover the lack of theoretical data and motivate experimentalist to investigate these further.

## 2 | METHOD OF CALCULATIONS

Full potential linearized augmented plane wave method written in FORTRAN language in Wien2k computational code[18] was utilized in present study. This method is taught to be excellent in term of calculation of structural, electronic, and optical properties.[19,20] Also maximum number of exchange correlation potential has been added to this method were integrated in Wien2k code. Within these potentials, we have applied Wu-Cohen[21] and Engle-Vosko[22] modified generalized gradient approximation (WC-GGA and EV-GGA) for the calculations of the article. WC-GGA was used for structural minimization and optimization while EV-GGA use taken in account for computation of electronic and optical properties. The scf file of EV-GGA was utilized in BoltzTraP code[23] for calculation of thermoelectric parameters. Some of analytical relations were used to calculate tolerance factor ($t$) (Equation (1)),[24] enthalpy of formation ($\Delta H$) (Equation (2)),[25] and lattice parameters (Equation (3))[26]

$$t = \frac{r_{Te} + r_{Rb/Cs}}{\sqrt{2}(r_{Cl} + r_{Te})} \quad (1)$$

$$\Delta H = E(Rb_2/Cs_2TeBr_6) - 2\left(E_{Cs/Rb}\right) - (E_{Te}) - 6(E_I) \quad (2)$$

$$E(V) = E_o + \frac{9V_oB}{16}\left[\left\{6 - 4\left(\frac{V_o}{V}\right)^{2/3}\right\}\left\{\left(\frac{V_o}{V}\right)^{2/3} - 1\right\}^2 + \left\{\left(\frac{V_o}{V}\right)^{2/3} - 1\right\}^3 B'\right] \quad (3)$$

In Equation (1), $r$ represents the radius of the respective atom in subscript, in Equation (2) each terms is the energy of unit cell or constituent atom in subscript while in Equation (3), $E_o$, $V_o$, $B$, $B'$, and $V$ are ground state energy, volume, bulk modulus, variation in bulk modulus with respect to pressure and variable volume, respectively.

## 3 | RESULTS AND DISCUSSION

### 3.1 | Structural properties

$Rb/Cs_2TeI_6$ compounds have $K_2PtCl_6$ type structure with Fm-3 m (#225) space group. Where, Rb/Cs atoms occupy (0.25, 0.25, 0.25) position, Te atom substitutes (0, 0, 0) position, and I atoms take (X, 0, 0). X is anion displacement parameters which is calculated by internal minimization technique and given in Table 1. The reliability of $Rb/Cs_2TeI_6$ compounds within cubic defective perovskite family was checked via calculating their tolerance factors ($t$) by relation given in Equation (1) by taken the ionic radii of constituent atoms from Reference 27. The

**TABLE 1** The elemental energies of Cs/Rb, Te, and I in bulk with ground stated energy and enthalpy of formation of $E(Rb_2/Cs_2TeI_6)$

| Parameter | $Rb_2TeBr_6$ | $Cs_2TeBr_6$ |
|---|---|---|
| $E_{Cs/Rb}$ | −81 080.61 | −211 873.32 |
| $E_{Te}$ | −184 853.11 | −184 853.11 |
| $E_I$ | −193 616.52 | −193 616.52 |
| $E(Rb_2/Cs_2TeI_6)$ | −1 508 727.69 | −1 770 312.527 |
| $\Delta H$ | −14.24 | −13.66 |

**TABLE 2** Present calculated lattice constant ($a_\circ$), volume ($V_\circ$), Bulk modulus ($B$), and its derivative with respect to pressure ($B'$), and anion displacement parameter ($X$) for $Rb/Cs_2TeI_6$ with available experimental (Exp.) and theoretical result

| Compound | $a_\circ$ (Å) | $V_\circ$(Å$^3$) | $B$ (GPa) | $B'$ | $X$ | Remarks |
|---|---|---|---|---|---|---|
| $Rb_2TeI_6$ | 11.5888 | 1554.44 | 20.58 | 5 | 0.2527 | Present |
| | 11.67 | | | | | Exp.[13] |
| $Cs_2TeI_6$ | 11.6423 | 1576.08 | 20.46 | 5 | 0.2522 | Present |
| | 11.70 | | | | | Exp.[14] |
| | 11.74 | | | | | Theo.[16] |
| | 11.7 | | | | | Theo.[17] |

calculate $t$ for $Rb_2TeI_6$ and $Cs_2TeI_6$ are 0.91 and 0.87, respectively. Therefore, $Rb/Cs_2TeI_6$ compounds are perovskites by condition $0.825 < t < 1.059$.[23]

A compound with negative enthalpy of formation ($\Delta H$) is termed as thermodynamically stable. To examine the stability of $Rb/Cs_2TeI_6$ compounds on basis of thermodynamics we have calculated the $\Delta H$ by fitting the data (ground state energies of $Rb/Cs_2TeI_6$ compounds and their constituent atoms) of Table 2 in Equation (2). The computed values are negative as seen from the table. These values guarantee the thermodynamic stability of the studied compounds.

In computational condense matter physics, Birch-Murnaghan's equation of state (Equation (3)) is used for calculation of structural parameters. Therefore, we have placed the data of volume optimization process in Equation (3) in order to get plots as in Figure 1. For which, we have selected the $V_\circ$, $B$, $B'$, and $E_\circ$ as constants. These constants (Table 1) are the computed structural parameters. The $B$ ($V_\circ$) of $Rb_2TeI_6$ is larger (smaller) than $Cs_2TeI_6$ because of comparatively smaller size of Rb than Cs. The lattice constant ($a_\circ$) was calculated from respective volume ($a_\circ = V^{1/3}$) and were found in excellent agreement with available result in experiment as clear from Table 1. The $a_\circ$ of $Cs_2TeI_6$ is larger than $Rb_2TeI_6$ because of larger volume.

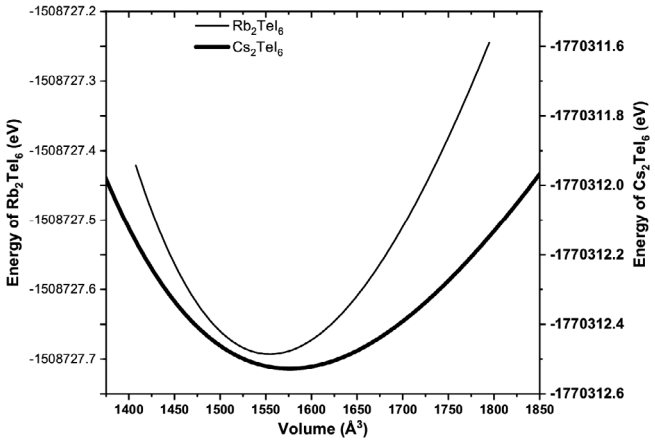


**FIGURE 1** Volume optimization plot for $Rb/Cs_2TeI_6$

## 3.2 | Electronic properties

The optical fitness of a material in solar cells and other related applications depend on its electronic properties. Therefore, we have calculated the electronic properties of $Rb/Cs_2TeI_6$ compounds via WC-GGA and EV-GGA in term of electronic band structure and density of states (DOS). Figure 2 contains only the band structures and DOS through EV-GGA because of similar response as by WC-GGA. The calculated band gaps ($W \rightarrow \Gamma$) through WC-GGA underestimates than experimental values while the values of EV-GGA little overestimates. However, the values of EV-GGA are in close resemblance with experimental values as clear from Table 3. We will use these values for calculation of optical and thermoelectric properties. The valence band maximum of both $Rb/Cs_2TeI_6$ compounds is flat. Hence, it is expected that both the compounds have excellent thermoelectric properties. In addition, optical properties are also expected to be better for solar cells and other optoelectronic properties. Because the DOS plots elaborate transition from I-5*p* states in valence band to Te-5*p* states in conduction band in case of both $Rb/Cs_2TeI_6$ perovskites.

## 3.3 | Optical properties

The optical fitness of a material to solar cell and optoelectronic applications can be deduced from important parameters such as real and imaginary parts of dielectric function (($\mathcal{E}_1(\lambda)$ and $\mathcal{E}_2(\lambda)$)), optical conductivity ($\sigma(\lambda)$) and refractive index ($n(\lambda)$). All these optical parameters were calculated as function of incident photon wavelength as depicted in Figures 3 and 4. Where, $Rb/Cs_2TeI_6$ compounds response to incident electromagnetic radiations in same way. As discussed above, that transition of charges take place between Te-5*p* and I-5*p* states when incident light is absorbed by $Rb/Cs_2TeI_6$ compounds. These states are speared in long range of conduction and valence bands. Therefore, despite low fundamental band gaps, $Rb/Cs_2TeI_6$ looks best for solar cell applications. To check this possibility, we calculated $\mathcal{E}_1(\lambda)$, $\mathcal{E}_2(\lambda)$, $\sigma(\lambda)$, and

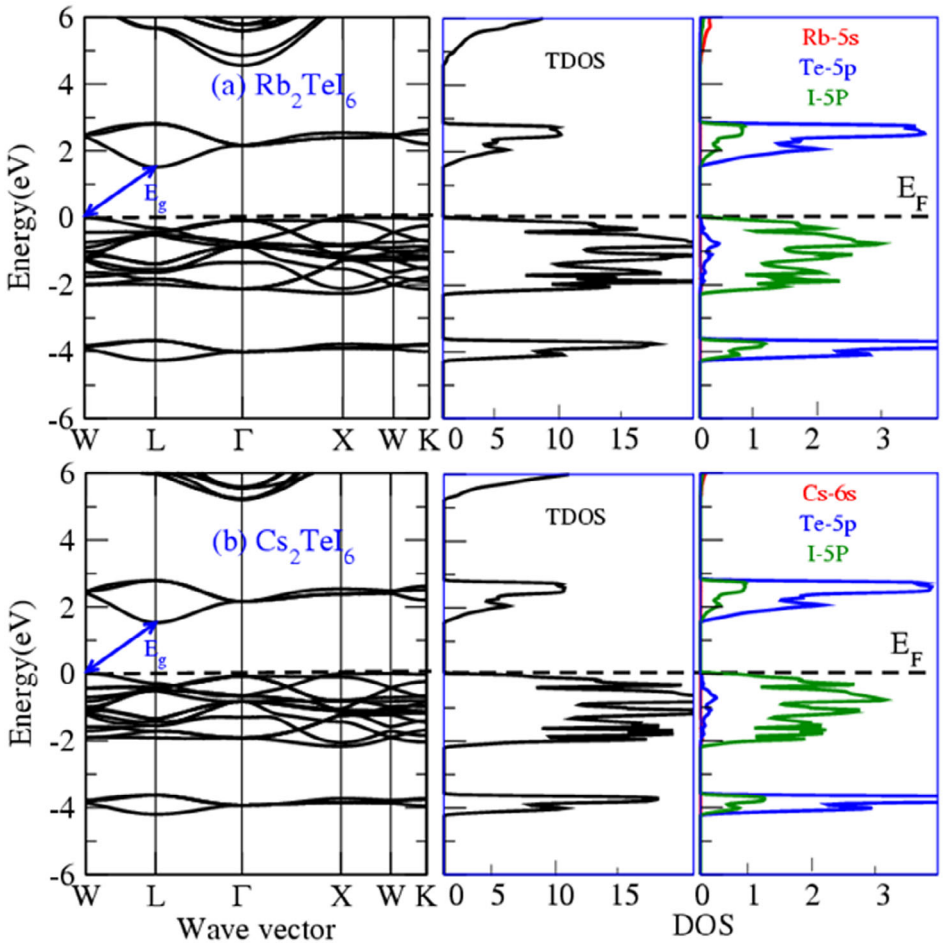


**FIGURE 2** The calculated electronic band structure with density of stated for, A, $Rb_2TeBr_6$ and, B, $Cs_2TeBr_6$ defective perovskites via EV-GGA [Colour figure can be viewed at wileyonlinelibrary.com]

**TABLE 3** Calculated band gaps through WC-GGA and EV-GGA along with experimental values

| Compound | Present (eV) | | Exp. (eV) |
|---|---|---|---|
| | WC-GGA | EV-GGA | |
| $Rb_2TeI_6$ | 1.321 | 1.482 | 1.4[15] |
| $Cs_2TeI_6$ | 1.344 | 1.521 | 1.5[15] |

$n(\lambda)$ in wavelength range of 250-750 nm as visible range is 400-700 nm.

Figure 3A elaborates the dispersion behavior of $Rb/Cs_2TeI_6$ in term of $\mathcal{E}_1(\lambda)$. At 250 nm, both the studied compounds have nearly zero dispersion. This value gets increase when wavelength of incident light increases. The maximum recorded value for $Rb_2TeI_6$ is 5.73 at 472 nm and for $Cs_2TeI_6$ is 5.69 at 496.7 nm wavelength. The values of $\mathcal{E}_1(\lambda)$ for both defective perovskites decrease linearly as the wavelength value increases and reaches to zero beyond red light.

$\mathcal{E}_2(\lambda)$ is used to describe the absorption ability of a materials when photons fall on it. The computed spectrum of $\mathcal{E}_2(\lambda)$ is shown in Figure 3B for $Rb/Cs_2TeI_6$ defective double perovskites. At 250 nm, both compounds have the value of $\mathcal{E}_2(\lambda)$ as 1. Beyond 250 nm, it increases and reaches to maximum value of 6.69 (at 443.7 nm) and 5.35 (at 463.1 nm) for $Rb_2TeI_6$ and $Cs_2TeI_6$, respectively. At 443.7 and 463.1 nm, minima peaks of $\mathcal{E}_1(\lambda)$ for $Rb_2TeI_6$ and $Cs_2TeI_6$, respectively, occur. It means that $Rb_2TeI_6$ has maximum absorption and less dispersion ability for violet light (380-450 nm) and $Cs_2TeI_6$ for blue light (450-495 nm). Overall, the enough good absorption in visible range makes both the compounds effective for solar cell applications.

The optical conductivity ($\sigma(\lambda)$) in Figure 3C follow the same trend in $\mathcal{E}_2(\lambda)$ in Figure 3B because absorption of light enables the charge carrier for conductance after getting transition of from valence to conduction band. The maximum values of $\sigma(\lambda)$ of 6431.9 ($\Omega^{-1}$ $cm^{-1}$) for $Rb_2TeI_6$ and 4932. 5 ($\Omega^{-1}$ $cm^{-1}$) for $Cs_2TeI_6$ take place at wavelengths for which maximum of $\mathcal{E}_2(\lambda)$ was observed. In entire taken range of wavelengths, the minimum values of $\sigma(\lambda)$ for both $Rb/Cs_2TeI_6$ compounds were observed for red light as clear from Figure 3B.

The refractive index $n(\lambda)$ measured for $Rb/Cs_2TeI_6$ perovskites is shown in Figure 3D. In regions 250-340 nm

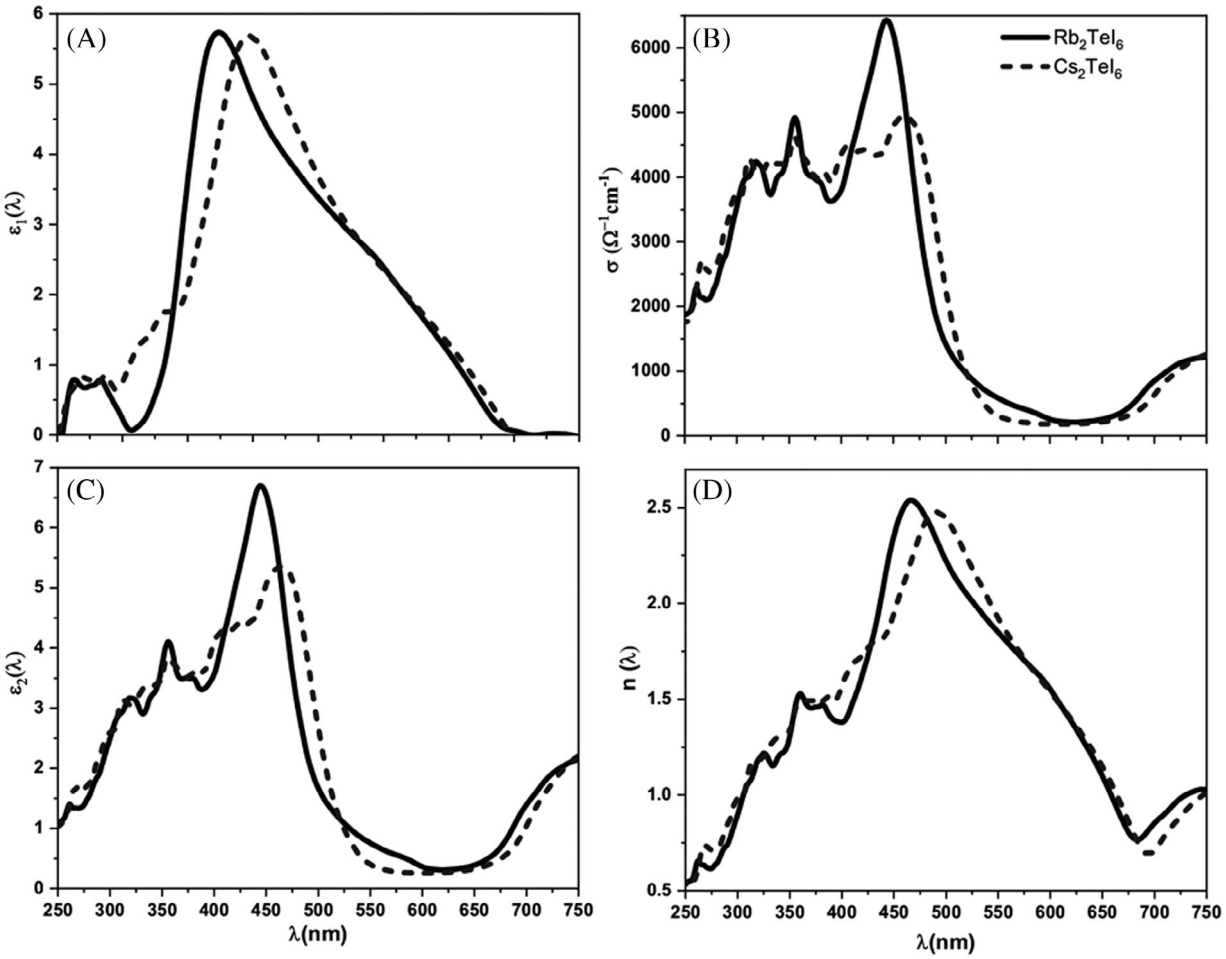


**FIGURE 3** Calculated real and imaginary parts of dielectric function (($\varepsilon_1(\lambda)$ and $\varepsilon_2(\lambda)$)), optical conductivity ($\sigma(\lambda)$), and refractive index ($n(\lambda)$) thermoelectric properties

and 660-750 nm, the $n(\lambda)$ has values lower than unity. In these regions, the phase velocity of the electromagnetic radiations exceeds the velocity of light ($v_p > c$) which looks to be nonphysical. In region 341-559 nm, the values of n greater than 1 reflects the transparent behavior of both the compounds. The maximum reported values of $n(\lambda)$ are 2.539 (at $\lambda = 466.8$ nm) for $Cs_2TeI_6$ and 2.477 (at $\lambda = 490.4$ nm) for $Rb_2TeI_6$.

## 3.4 | Thermoelectric properties

The $Rb/Cs_2TeI_6$ compounds were investigated for thermoelectric power generation in term of, total thermal conductivity ($\kappa$) along with its electronic ($\kappa_e$) and lattice parts ($\kappa_L$), electronic conductivity ($\sigma/\tau$), Seebeck coefficient ($S$), power factor ($PF/\tau$), and figure of merit ($ZT$) in temperature range of 100-1000 K and summarized in Figures 4 to 6. All these parameters except $\kappa_L$ were calculated through BoltzTraP code while the calculation of $\kappa_L$ was carried out using Slack equation.[28]

Figure 4A-C depicts the computed $\kappa_e$, $\kappa_L$, and $\kappa$, respectively. $\kappa_e$ is measure of electronic part in heat transfer. Its value increases with increase in temperature for semiconductors. Figure 4A is evidence of this statement. Where, $\kappa_e$ increases from $0.147 \times 10^{14}$ to $8.19 \times 10^{14}$ W/mKs for $Rb_2TeI_6$ and $0.148 \times 10^{14}$ to $7.91 \times 10^{14}$ W/mKs for $Cs_2TeI_6$. Figure 4B shows phonon contribution (lattice thermal conductivity, $\kappa_L$) to heat transfer calculated via Slack equation.[28]

$$\kappa_L = A\frac{\Theta_D^3 V^{\frac{1}{3}} M_{avg}}{\gamma^2 n^{\frac{2}{3}} T\tau} \quad (4)$$

In Equation (4), $\gamma$ is the Grüneisen parameter, $A$ is $\gamma$ dependent coefficient ($\sim 3.1 \times 10^{-6}$ for $\kappa_L$ in W/mKs),[29] $V$ is the volume (in unit of Å$^3$) per primitive unit cell, $M$ is the average atomic mass (in unit of amu) of all the atoms, $\tau$ is relaxation time ($10^{-14}$ seconds), $T$ is the temperature in K, $\Theta_D$ is Debye temperature in $K$, and $n$ is the total number of atoms in primitive unit cell. $\Theta_D$ (153.35

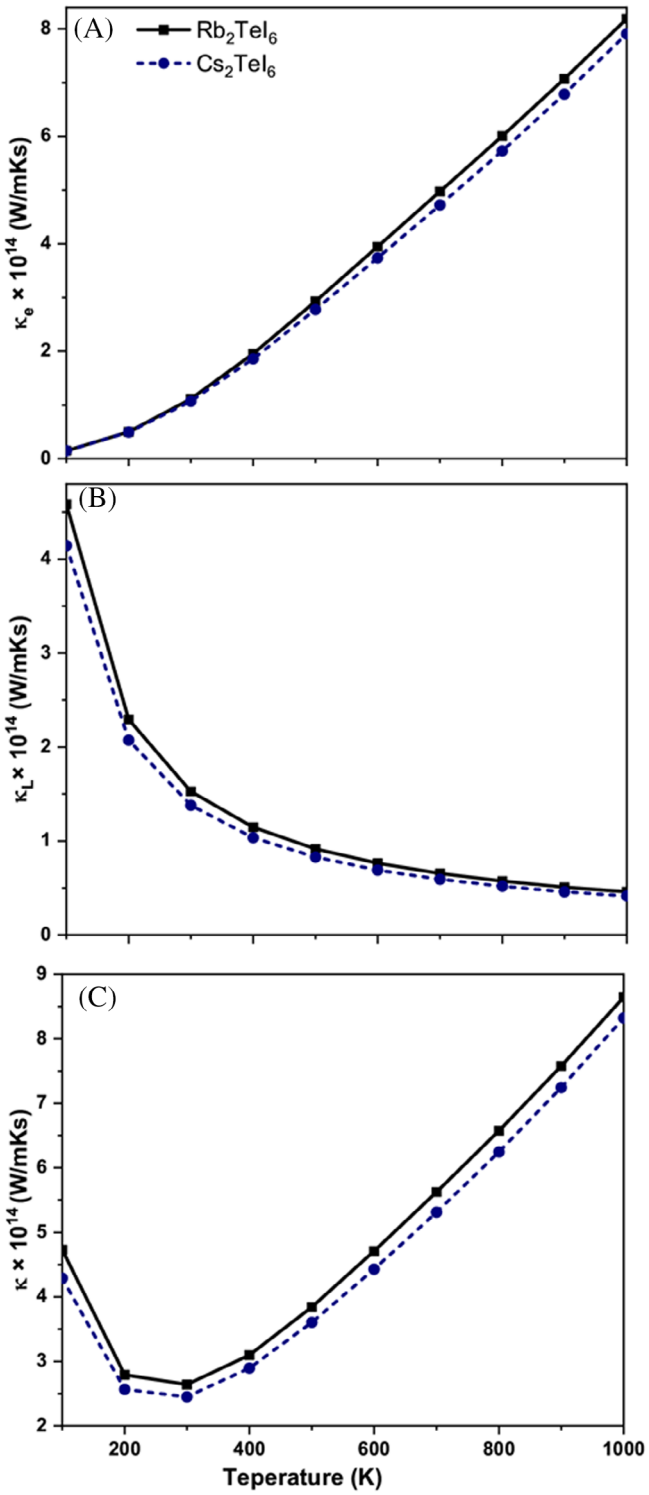


**FIGURE 4** Calculated, A, electronic ($\kappa_e$), B, thermal ($\kappa_L$), and, C, total ($\kappa$) thermal conductivities of $Rb/Cs_2TeI_6$ compounds [Colour figure can be viewed at wileyonlinelibrary.com]

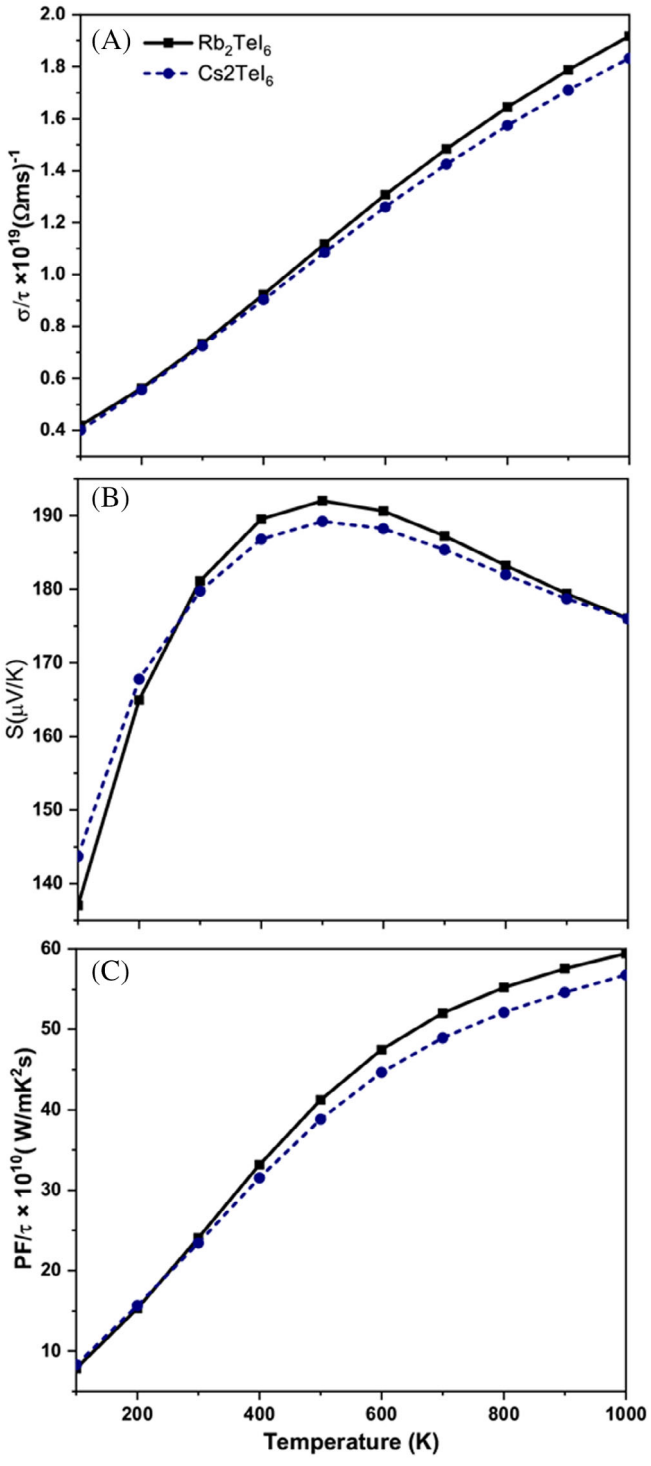


**FIGURE 5** The calculated, A, electronic conductivity ($\sigma/\tau$), B, Seebeck coefficient ($S$), and, C, power factor ($PF/\tau$) and for Rb/Cs2TeI6 defective perovskites [Colour figure can be viewed at wileyonlinelibrary.com]

for $Rb_2TeI_6$ and 148.01 for $Cs_2TeI_6$) and $\gamma$ (2.35 for both $Rb/Cs_2TeI_6$ compounds) are calculated through Quasi-harmonic Debye approximation.[30] Figure 4B specifies that $\kappa_L$ decreases with rise in temperature. When temperature rises, the inter-atomic lattice chain becomes weaker. This causes a decrease in phonon group velocity and hence in $\kappa_L$. The total thermal conductivity ($\kappa = \kappa_e + \kappa_L$) is depicted in Figure 4C. Both the $Rb/Cs_2TeI_6$ compounds show

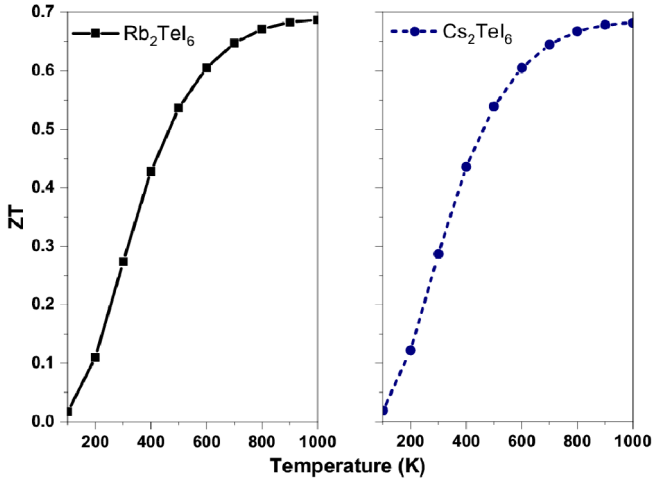


**FIGURE 6** The computed figure of merits (*ZT*) for Rb/Cs2TeI6 defective perovskites [Colour figure can be viewed at wileyonlinelibrary.com]

similar behavior. Up to room temperature, $\kappa$ decreases and then increases with further rise in temperature. This is justified by respective values of $\kappa_e$ and $\kappa_L$.

Figure 5A shows the calculated relaxation time dependent electronic conductivity ($\sigma/\tau$). Where, $\sigma/\tau$ is nearly linear relationship with temperature. This type behavior is common for semiconductor type materials.[31] Because, an increase in temperature causes decrease in resistance in a semiconductor, as result the charges conductivity rises. The maximum values of $\sigma/\tau$ were noted at 1000 K as $1.92 \times 10^{19}$ $(\Omega ms)^{-1}$ for $Rb_2TeI_6$ and $1.83 \times 10^{19}$ $(\Omega ms)^{-1}$ for $Cs_2TeI_6$.

The *S* in Figure 5B shows the same behavior for $Rb/Cs_2TeI_6$ compounds throughout entire temperature range. Initially, its values increase up to 500 K and then decrease linearly with rise in temperature. The maximum value was calculated for 192.01 V/mK for $Rb_2TeI_6$ and 189.24 V/mK for $Cs_2TeI_6$ at 500 K. In addition, the positive values of *S* in whole temperature range specify the studied compounds as p-type semiconductors.

Power factor $PF/\tau = \sigma S^2/\tau$[32] varies with temperature change as shown in Figure 5C. The values of $PF/\tau$ for both perovskites increase linearly up to 500 K and then increase is comparatively smooth. Maximum values of PF/τ for reference in future works are $59.42 \times 10^{10}$ and $56.76 \times 10^{10}$ $Wm/K^2s$, respectively, for $Rb_2TeI_6$ and $Cs_2TeI_6$. The increase of $PF/\tau$ with rise in temperature makes $Rb/Cs_2TeI_6$ compounds as thermoelectric potential materials.

A dimensionless quantitative, figure of merit (*ZT*) describes the efficiency of material to convert heat in electrical energy. The *ZT* for $Rb/Cs_2TeI_6$ perovskites as function of temperature is shown in Figure 6. The maximum values of *ZT* are reported as 0.687 for $Rb_2TeI_6$ and 0.682 for $Cs_2TeI_6$ at 1000 K. In wide range conditions, the *p*-type $Rb/Cs_2TeI_6$ perovskites with good *ZT* values as novel materials for efficient thermoelectric devices.

## 4 | CONCLUSIONS

The density functional theory employed in wien2k computational code was used to investigate structural, electronic, optical and thermoelectric properties of $Rb/Cs_2TeI_6$ defective perovskites. The bulk modulus and enthalpy of formation provide as reference data. In addition, the negative values of enthalpy of formation confirmed the thermodynamic stability of both the compounds. The band gaps calculated through EV-GGA were found in close agreement with experimental values. From density of states calculations, it was explored that band gap is attributed by Te-5*p* states in conduction band and I-5*p* states in valence band. The excellent absorption and conductance in visible region of electromagnetic spectrum ensured the commercial use of lead free $Rb/Cs_2TeI_6$ compounds in solar cell applications. Also, the calculated reasonable values of electronic conductivity, Seebeck coefficient, power factor, and figure of merit make *p*-type $Rb/Cs_2TeI_6$ perovskites favorable for thermoelectric power generation.

## ACKNOWLEDGEMENT

Murefah mana AL-Anazy extended her sincere appreciation to the Deanship of Scientific Research at Princess Nourah Bint Abdulrahman University through the Fast-track Research Funding Program.

## DATA AVAILABILITY STATEMENT

Data sharing not applicable to this article as no datasets were generated or analyzed during the current study (the article describes entirely theoretical research).

## ORCID

*Malak Azmat Ali* https://orcid.org/0000-0002-6290-0317
*Ali H. Reshak* https://orcid.org/0000-0001-9426-8363
*Ghulam Murtaza* https://orcid.org/0000-0001-5520-2265

## REFERENCES

1. Laboratory NRE. Best research-cell efficiency chart. 2019. https://www.nrel.gov/pv/cell-efficiency.html.
2. Kosnett MJ, Wedeen RP, Rothenberg SJ, et al. Recommendations for medical management of adult lead exposure. *Environ Health Perspect*. 2007;115(3):463-471.

3. Song Z, Abate A, Watthage SC, et al. Perovskite solar cell stability in humid air: partially reversible phase transitions in the $PbI_2$-$CH_3NH_3I$-$H_2O$ system. *Adv Energy Mater*. 2016;6:1600846.
4. Ullah R, Ali MA, Murtaza G, Khan A, Mahmood A. Ab initio study for the structural, electronic, magnetic, optical, and thermoelectric properties of $K_2OsX_6$ (X = Cl, Br) compounds. *Int J Energy Res*. 2020;44:9035-9049.
5. Mahmood Q, Gharib T, Rached A, Laref A, Kamran MA. Probing of mechanical, optical and thermoelectric characteristics of double perovskites $Cs_2GeCl/Br_6$ by DFT method. *Mater Sci Semicond Process*. 2020;112:105009.
6. Huma M, Rashid M, Mahmood Q, Algrafy E, Kattan NA. Physical properties of lead-free double perovskites $A_2SnI_6$ (A = Cs, Rb) using ab-initio calculations for solar cell applications. *Mater Sci Semicond Process*. 2021;121:105313.
7. Ullah R, Ali MA, Murtaza G, Mahmood A, Ramay SM. The significance of anti-fluorite $Cs_2NbI_6$ via its structural, electronic, magnetic, optical and thermoelectric properties. *Int J Energy Res*. 2020;44:1-13. https://doi.org/10.1002/er.5638.
8. Lee B, Krenselewski A, Baik SI, Seidman DN, Chang RPH. Solution processing of air-stable molecular semiconducting iodosalts $Cs_2SnI_{6-x}Br_x$, for potential solar cell applications sustainable. *Energy Fuel*. 2017;1(4):710-724.
9. Maughan AE, Ganose AM, Bordelon MM, Miller EM, Scanlon DO, Neilson JR. Defect tolerance to intolerance in the vacancy-ordered double perovskite semiconductors $Cs_2SnI_6$ and $Cs_2TeI_6$. *J Am Chem Soc*. 2016;138:8453-8464.
10. Lee B, Stoumpos CC, Zhou NJ, et al. Metal-free tetrathienoacene sensitizers for high-performance dye sensitized solar cells. *J Am Chem Soc*. 2014;136:15379-15385.
11. Murtaza G, Hussain S, Faizan M, Khan S, Algrafy E, Ali MA. Anion-cation replacement effect in lead free tin based variant perovskites. *Physica B Condens Matter*. 2020;595:412345.
12. Kapil G, Ohta T, Koyanagi T, et al. In situ construction of a $CS_2SNI_6$ perovskite nanocrystal/$SNS_2$ nanosheet heterojunction with boosted interfacial charge transfer. *J Phys Chem C*. 2017;121:13092-13100.
13. Abriel W. Crystal structure and phase transition of $Rb_2TeI_6$. *Mater Res Bull*. 1982;17:1341-1346.
14. Sidey VI, Zubaka OV, Solomon AM, Kun SV, Peresh EY. X-ray powder diffraction studies of $Tl_2TeBr_6$ and $Tl_2TeI_6$. *J Alloys Compd*. 2004;367:115-120.
15. Peresh EY, Zubaka OV, Sidei VI, Barchii IE, Kun SV, Kun AV. Preparation, stability regions, and properties of $M_2TeI_6$ (M = Rb, Cs, Tl) crystals. *Inorg Mater*. 2002;38:1020-1024.
16. Brik MG, Kityk IV. Modeling of lattice constant and their relations with ionic radii and electronegativity of constituting ions of $A_2XY_6$ cubic crystals (A=K, Cs, Rb, Tl; X=tetravalent cation, Y=F, cl, Br, I). *J Phys Chem Solids*. 2011;72:1256-1260.
17. Rahim W, Cheng A, Lyu C, et al. Geometric analysis and formability of the cubic $A_2BX_6$ vacancy-ordered double perovskite structure. *Chem Mater*. 2020;32(2020):9573-9583.
18. Bhala P, Schwarz K, Tran F, Laskowski R, Madsen GKH, Marks DL. WIEN2k: an APW+lo program for calculating the properties of solids. *J Chem Phys*. 2020;152:074101.
19. Chadli A, Halit M, Lagoun B, et al. Structural and anisotropic elastic properties of hexagonal $YMnO_3$ in low symmetry determined by first-principles calculations. *Solid State Phenom*. 2019;297:120-130.
20. Al-Qaisi S, Ahmed R, Haq BU, Rai DP, Tahir SA. A comprehensive first-principles computational study on the physical properties of lutetium aluminum perovskite $LuAlO_3$. *Mater Chem Phys*. 2020;250:123148.
21. Wu Z, Cohen RE. More accurate generalized gradient approximation for solids. *Phys Rev B*. 2006;73:235116.
22. Engle E, Vosko SH. Exact exchange-only potentials and the virial relation as microscopic criteria for generalized gradient approximations. *Phys Rev B*. 1993;47:13164-13174.
23. Madsen GKH, Singh DJ. BoltzTraP. A code for calculating band-structure dependent quantities. *Comput Phys Commun*. 2006;175:67-71.
24. Bartel CJ, Sutton C, Goldsmith BR, et al. New tolerance factor to predict the stability of perovskite oxides and halides. *Sci Adv*. 2019;5:eaav0693.
25. Ali MA, Murtaza G, Laref A. Exploring ferromagnetic half-metallic nature of $Cs_2NpBr_6$ via spin polarized density functional theory. *Chin Phys B*. 2020;29:066102.
26. Murnaghan FD. The compressibility of media under extreme pressures. *Proc Natl Acad Sci U S A*. 1944;30:244-247.
27. Amar MN, Ghriga MA, Seghier MEAB, Ouaer H. Prediction of lattice constant of $A_2XY_6$ cubic crystals using gene expression programming. *J Phys Chem B*. 2020;124:6037-6045.
28. Slack GA. The thermal conductivity of nonmetallic crystals. *Solids State Phys*. 1979;34:1.
29. Morelli DT, Jovovic V, Heremans JP. Intrinsically minimal thermal conductivity in cubic I–V–VI2 semiconductors. *Phys Rev Lett*. 2008;101:035901.
30. Blanco MA, Francisco E, Luania V. GIBBS: isothermal-isobaric thermodynamics of solids from energy curves using a quasiharmonic Debye model. *Comput Phys Commun*. 2004;158:57-72.
31. Shah SH, Murtaza G, Baz A, Algrafy E, Laref A, Kattan NA. Study of anion replacement effect on $SrCd_2X_2$ (X = P, As, Sb, Bi) compounds by FPLAPW+lo. *Mater Sci Semicond Process*. 2020;119:105290.
32. Hong AJ, Li L, He R, et al. Full-scale computation for all the thermoelectric property parameters of half-Heusler compounds. *Sci Rep*. 2016;6:22778.


**How to cite this article:** Ali MA, Reshak AH, Murtaza G, et al. Optoelectronic and transport properties of $Rb/Cs_2TeI_6$ defective perovskites for green energy applications. *Int J Energy Res*. 2020; 1–8. https://doi.org/10.1002/er.6378